DESERT

Desert
Online at http://desert.ut.ac.ir

Desert 25-1 (2020) 77-85

Evaluating different spectral indices in identification and preparation of soil salinity mapping of arid region of Iran

H.R. Matinfar[a*], A. Fariabi[b], S.K. Alavipanah[b]

[a] *Lorestan University, Khorramabad, Loresan, Iran*
[b] *RS & GIS Dept., Faculty of Geography, University of Tehran, Tehran, Iran*

Received: 30 May 2019; Received in revised form: 18 February 2019; Accepted: 19 February 2019

Abstract

Soil salinity undergoes significant spatial and temporal variations; therefore, salinity mapping is difficult, expensive, and time consuming. However, researchers have mainly focused on arid soils (bare) and less attention has been paid to halophyte plants and their role as salinity indicators. Accordingly, this paper aimed to investigate the relationship between soil properties, such as electrical conductivity of the saturation extract (ECe) and the spectral reflectance of vegetation species and bare soil, to offer a method for providing salinity map using remote sensing. Various vegetation species and bare soil reflectance were measured. Spectral Response Index (SRI) for bare soil and soil with vegetation was measured via the Normalized Difference Vegetation Index (NDVI), Soil Adjusted Vegetation Index (SAVI), and salinity indexes. The electrical conductivity of the saturated extract, texture, and organic matter of soil samples were determined. The correlation coefficient of soil salinity with SRI, SAVI, and salinity indexes were obtained, and a model was presented for soil salinity prediction. EC map was estimated using the proposed model. The correlation between SRI and EC was higher than other models (0.97). The results showed that the salinity map obtained from the model had the highest compliance (0.96) with field findings. In general, in this area and similar areas, the SRI index is an acceptable indicator of salinity and soil salinity mapping.

Keywords: Spectral indices; Soil salinity; SRI; Vegetation index

1. Introduction

The traditional method of salinity deduction from other soil properties as well as visual interpretation of aerial photographs have been employed to monitor and collect data to show salinity. Mapping salinity with aerial photo interpretation is limited to distinctive signs of visually-identifiable salinity. Interpretation of aerial photographs together with soil landscape map has resulted in the identification of soil salinity among different soil properties, soil landscape map location, and a number of field samples. Each map unit may comprise various soil properties and salinity, but the exact location and extent of salinity in the map units is not perceptible (Nasir khan *et al*., 2005).

* Corresponding author. Tel.: +98 912 3450969
Fax: +98 66 33431917
E-mail address: matinfat.h@lu.ac.ir

Indices employing Green, Red and Near-Infrared bands of Landsat TM and OLI have been showed agood correlation with the measured EC value in Ethiopia and Saudi Arabia [(Elhag, 2016. Asfaw *et al*, 2016)]. Morshed *et al*. (2016) studied the potential of Landsat ETM+ for detecting soil salinity of the coastal region of Bangladesh. In that study. Thirteen indices have been employed to find out the relationship between indices and salinity values collected from the field. A regression equation has been developed from the analysis which is capable of mapping the saline affected areas from Landsat ETM+ images (Morshed *et al*, 2016). But there is a research gap in case of soil salinity mapping for Bangladesh using Landsat TM.

Over the past two decades, multispectral satellite images have been used for mapping and monitoring surface salinity in several studies (Hick and Russell, 1988; Furby *et al*., 1995, 1998; Metternicht and Zinck, 2003). Preparation of direct saline soil maps using broadband

satellite images is associated with major issues in saline soil areas covered by salt-tolerant species (Howari, 2003; Furby *et al.*, 1995). The same problem was also observed in soils without salt crusts (Howari, 2003). Furby *et al*. (1995) observed that non-saline sandy soil surfaces, sometimes severely incorrectly interpreted with affected by areas of saline free of vegetation; in other words, there was spectral interference. Most studies have attempted to overcome the limitations of spectral-spatial images by combining multitemporal images with auxiliary information such as soil data and land properties (Furby *et al.*, 1995, 1996; Kiiveri and Caccetta 1998; Caccetta *et al*., 2000; Thomas 2001, Fernandez-Buces *et al*., 2006).

When the soil is bare, land surface salinity can be directly distinguished using remote sensing data whilein vegetated lands, it can be specified by the type of vegetation and the growth conditions controlled by salinity (Mougenot *et al*., 1994). Surface salinity is an active process affecting the spectral and spatial information extracted from conventional data. Identification of saline soils by remote sensing data is largely dependent on humidity, salinity rate, crust type, and the contrast of saline spectral reflectance with other surfaces. In general, areas with medium and high salinity have been more successfully identified compared to those with low salinity or in the early stages of salinization. For example, McGowen and Mallyon (1996), using TM data and maximum likelihood classification algorithm, provide more saline areas estimation more than expected, which was due to the land management, vegetation conditions, and soil type of the studied area.

However, the remote sensing approach to mapping at regional scales still requires development for the purposes of global agricultural salinization. One substantial challenge is to resolve a large mismatch between the scales of the ground and satellite measurements. In addition, the direct assessment of soil salinity from bare soil reflectance is limited in regard to a salinity of lower than 20 dSm^{-1} (Metternicht and Zinck, 2003; Allbed *et al*., 2018).

On the contrary, remote sensing can minimize the time and cost for broad sampling and salinity mapping because salinity levels are assessed by various band reflectances and satellite imagery ratios (Tamȷs and Lénȷrt, 2006; Eldeiry and Garcia, 2008).

This problem is solved combining multitemporal images. On the other hand, the salinity level estimated lower than expected, by remote sensing, is due to the mixture of saline soils with nonsaline ones (Zinck, J. A. 2001). However, the identification of saline soils can be improved by combining multi-spectral data with field studies and GIS. El Hafyani (2019) modeled and mapped soil salinity in Tafilalet plain, Morocco, based on Landsat 8 OLI satellite data in combination with ground field data. His results showed that the coefficient of determination (R2) varied from 0.53 to 0.75 and the Root Mean Square Error (RMSE) ranged between 0.62 and 0.80 dS/m.

Yan *et al*. (2019) used proximal sensor data for soil salinity management and mapping and reported that there was limited information concerning spatio-temporal variations of soil salinity in the study areas. Such information is necessary for mapping changes in saline areas and identifying appropriate strategies for soil salinity management. Yan *et al*. (2019) Stated, EM38 data were used for digital soil mapping of spatio-temporal variations in different regions. The results showed that the soil salinity distribution was heterogeneous in the middle, and salt leaching was significant at its edges.

Mougenot (1993) holds that broadband multi-spectral satellite images (Landsat, SPOT) have limited ability to check for saline-affected areas, especially when the amount of salt in the soil is less than 10-15%. Farifteh *et al*. (2006) determinedthree types of variables, called measurable, hidden, and computational, for the zoning of saline soils based on remote sensing. Other complications as well as vegetation interference in reflectance production create errors in identifying the salinity (Alavi Panah *et al*., 1999, 2001). They believe that the contribution of remote sensing tools depends on the number of hidden variables compared to the other tools. Furthermore, if the behavior of the system under study completely follows hidden variables, it is less likely that the remote sensing data can provide useful information. Spatial resolution of images is another factor affecting the zoning accuracy. Broadband satellite sensors utilized in identifying saline soils are TM, MSS, SPOT XS, Terra-ASTER, and LISS-II/III.

Dwivedi *et al*. (1998) performed zoning in Indo-Gangetic saline land plains using LISS_III sensor images of IRS-1C satellites and a color transfer function of intensity, hue, and saturation with a zoning accuracy of more than 85%.

Ahmed and Andriana Solo (1997) compared the performance of Landsat TM and SPOT XS for the saline soil zoning in a semi-comparative level. They observed that SPOT XS had a better performance compared with Landsat TM whilethe distinction between areas with moderate salinity levels and high eroded levels

with relaxants was difficult due to the same spectral reflectance. Verma *et al.* (1994) demonstrated that the combination of thermal bands such as TM6 or ETM6 with NIR-VIS bands was effective in reducing the similarity between Spectral properties of saline soils. Shaya *et al*. (2005) identified salt-affected areas with dominated sodium chloride salts and sodium sulfate on Aibi lake area in China using ASTER image. They reported a good correlation between the concentration of surface salts and band 1 (green) ASTER images, followed by red and infrared bands.

Remote sensing uses the electromagnetic energy reflected from targets to obtain information on the earth's surface (Khorram *et al*., 2012). Because soil salinity impacts vegetation, remotely sensed vegetation reflectance can be used as an indirect indicator of soil salinity (Metternicht and Zinck, 2008; Zhang *et al*., 2011).

Similar results were obtained by Brunner *et al*. (2004) on preparing non-calibrated salinity mapping using atmospheric multispectral ASTER images correction. Non-calibrated salinity maps generated via spectral correction are comparable to the average conductance values obtained from ground-based measurements. Dwivedi *et al*.(2001)conducted a comparative study on the performance of IKONOS multispectral images and LISS-III sensor of IRS-1D satellite data with panchromatic (spatial resolution of 5.8 m) and multi-spectral (spatial resolution of 23.5 m) for the zoning of saline soils.

Using different classification methods and image conversion while employing IKONOS data, a total accuracy of 92.4% was obtained. In contrast, using the multi-spectral LISS-III data and the combination of multi-spectral data and panchromatic LISS-III, the total accuracy were 78.4% and 84.3%, respectively. Lands covered with vegetation and agricultural crops are among the limitations of mapping salt-affected soils. Some physiological and environmental responses of plants to the electromagnetic spectrum cause the use of spectral behavior of plants in the study of vegetation.

Moreover, Normalized Difference Vegetation Index (NDVI) derived from the plant reflects red and near-infrared wavelengths can represent spectral behavior of plants (Nagler *et al*., 2001). This index shows a positive correlation with plant photosynthesis activities, plant biomass, and leaf area index (LAI);on the other hand, they have been proven effective in determining the distribution pattern of plants and their response to environmental factors such as salinity. The spatial resolution of satellite imagery is an important factor that should be considered when mapping and assessing soil salinity (Ben-Dor *et al*., 2008; Schmid *et al*., 2008).

Reflection spectrum of bare soil and plant species vary in their salinity conditions. Thus, It must be possible for soil mapping algorithm using spectral reflectance of bare soil and vegetation as an indicator. In this study, spectral indices derived from Landsat TM and field studies were integrated, and soil salinity map was then prepared based on the fitted model on spectral and field data.

2. Materials and Methods

2.1. Study area

The study area was the Ravand plain (Figure 1) with hot and relatively long summers and mild winters. Based on the metrological data of 30 years, the mean annual precipitation is 138.8 mm with annual evapotranspiration potentials above 2000 mm. Rainy time's start from November and end in June. Based on meteorological data, soil temperature regime is thermic with an aridic moisture regime. According to previous studies and surveys, the soils of this region are classified into Entisols and Aridisols.

2.2. Data

Landsat TM image bands on July 3, 2016, included the visible spectrum (blue, green, and red), reflected infrared (NIR and MIR), and thermal infrared. Topographic maps, soil, and salinity map at the scale of 1:50000, ENVI5.3, ArcGIS10, and SPSS18 software were used.

2.3. Field data

Based on the visual interpretation of TM432 false color composite, areas of image with homogeneous color, texture, and uniformity were selected as a unit. Afterwards, 5 to 10 random samples were selected within each homogeneous unit with a depth of zero to 30 cm, with at least one profile per unit. Dried and sieved samples, mmeasuring salinity values, soil reaction, lime, soil color, and organic matter according to standard laboratory methods. Plants in each homogeneous region were identified, and the frequency and types were also determined. Native plants in the study area comprise *Petropyron* sp., *Hultemia* sp., *Launaed* sp., *Alhagi comelorum*, *Euphorubia* sp., *Salsola tomentosa*, and *Heltemia* sp. Dominant crops are corn, cotton, and barley.

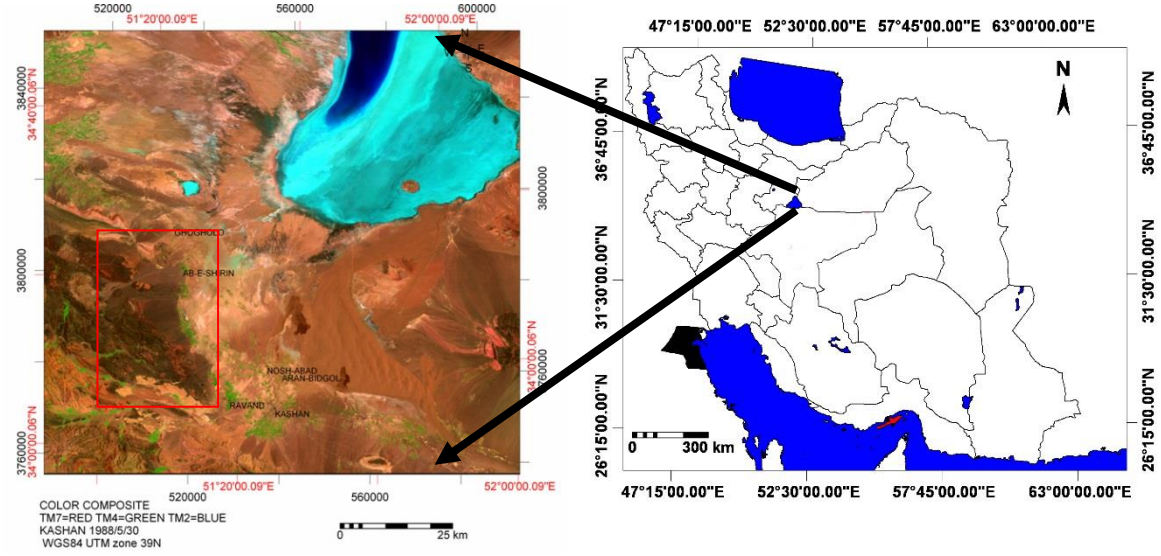

Fig. 1. Location of the study area, Iran

2.4. Data processing

Using 14 ground control points, next, the parameters of UTM projection, zone 39, WGS 84 spheroid, and datum were defined. Radiometric correction was performed using least histograms. The color of several plants and bare soil was determined at 104 sampling points. NDVI was calculated for all samples using TM images of dereferenced pixel size 30 m. Three bands (blue (1), green (2), and red (3)) and a fourth band, near infrared (NIR), were extracted. After that, Pearson correlation coefficient (r) was calculated for the relationship between NDVI and EC. Several algorithms of bands 4-1 in combination with NDVI were tested to extract bare soil reflection and find the most optimal correlation with soil EC. Data integration algorithm, called Spectral Response Index (SRI), determines a combination of bare soil and vegetation spectral responses (Fernandez Bosez *et al*., 2006). Regression relationships were studied to obtain an equation able to predict EC from spectral indices such as SI, BI, and SRI (Table2). When a significant relationship was found between SI, BI, SRI and soil EC. Statistical analysis was performed by means of Minitab16 and SPSS 18 software.

3. Results and Discussion

The results of analysis showed that soilsalinity varied from 2 to 105 dS / m with a pH of 7.1 to 8.7 (Table 1). Soil salinity class ranged from S0 to S6, indicating the variety of vegetation and soils on one hand and the variety of plant species on the other. Soil texture varied from loam to sandy loam, confirming medium to high permeability and low water storage capacity. Arid climate can cause sparse vegetation and the growth of drought and salinity-resistant plants in the area. The results of field studies confirmed the sparseness of pasture vegetation, which were salt-tolerant species.

Table 1. Results of physic-chemical properties measurements on some control sites

Site NO.	Sand (%)	Silt (%)	Clay (%)	OC (%)	CaCO3 (%)	CaSO4. 2H2O (%)	Ec (dS/m)	pH	SP%	Sampling depth (cm)
3	52.00	30.00	18.00	0.36	17.50	0.00	1.20	8.31	24.10	0.30
7	32.00	38.00	30.00	0.50	20.30	0.00	3.71	8.27	30.00	0.30
11	34.00	30.00	36.00	0.23	10.50	9.00	3.53	8.11	44.20	0.30
19	59.00	27.00	14.00	0.28	10.20	9.00	74.8	7.80	33.8	0.30
24	73.80	12.40	13.80	0.28	13.70	22.00	89.80	7.95	40.00	0.30
32	44.00	33.00	23.00	0.45	16.50	3.50	105.60	8.27	32.50	0.30
40	59.00	25.00	16.00	0.65	17.50	4.60	82.80	7.65	30.30	0.30

A two-dimensional scatter plot of image pixels were drawn to identify the land cover distribution. NDVI index and two-dimensional graph properly displayed the vegetation distribution of bare soils, pasture vegetation, and irrigated agriculture in the study area (Figures 1 and 2). As shown in Figure 1, saline soils were light to gray, and vegetation was red. The distribution of image pixels was triangular, the pixels around the triangle represent lush green

vegetation and the base pixels represent bare soil. The base pixels of the triangle near the origin represent dark soil and the front represents light colored soils as saline crust and saline soil. (Figure 2b).

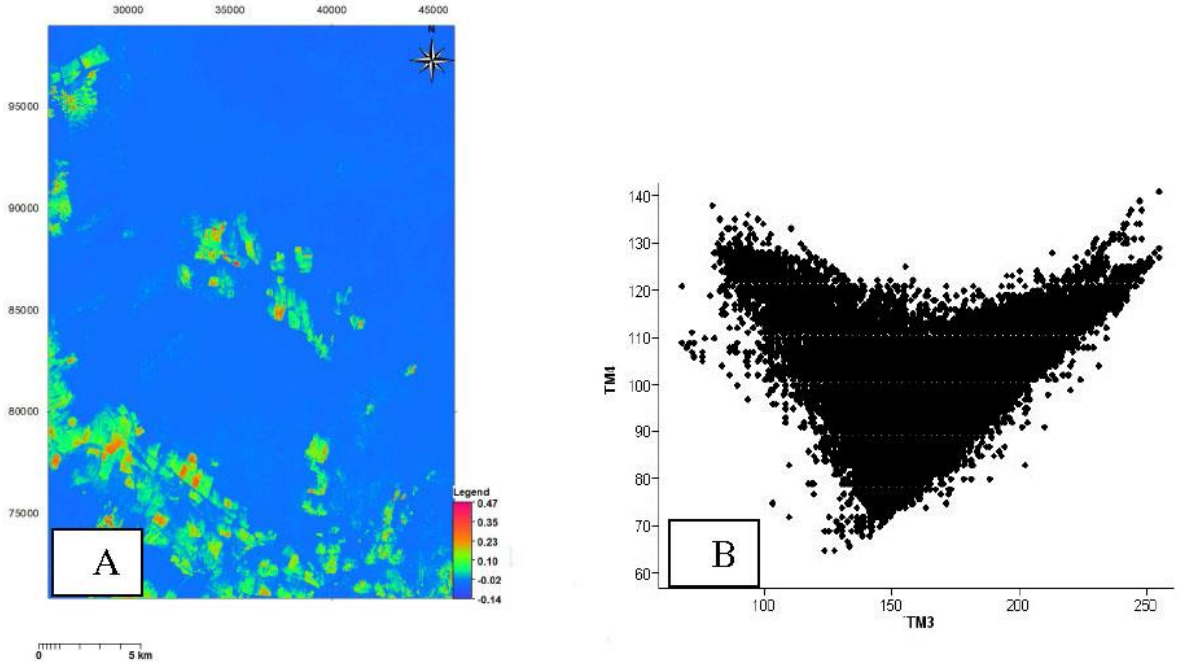

Fig. 2. a) NDVI index calculated for the study area, b) scatter plot of R and NIR spectral band

As shown in Figure 2b, there was no vegetation in the northern area, In the west and south, scattered masses of irrigated agriculture and rainfed agriculture and in the central region, masses of planted trees are distributed.Spectral indices of plant, soil, brightness, and salinity were determined using blue, green, red, and near infrared band of the TM sensor and their correlation with measured salinity was determined by laboratory method (Table 2).

Table 2. Spectral indexes and correlation with measured soil salinity

Indexes	Formula	R2
Soil Adjusted Vegetation Index(SAVI)	(NIR-R)*L/(NIR+R+L)	0.29
Normalized Difference Salinity Index(NDSI)	(R-NIR)/(R+NIR)	0.36
Brightness Index1(BI1)	$\sqrt{(NIR^2+R^2)}$	0.43
Brightness Index1(BI2)	$\sqrt{(NIR^2+G^2)}$	0.38
Vegetation Soil Salinity Index(VSSI)	2*G-5*(R+NIR)	0.39
Salinity Index1(SI1)	√(B*R)	0.41
Salinity Index2(SI2)	√(G*R)	0.39
Salinity Index3(SI3)	√(NIR2+R2+G2)	0.45
Salinity Index4(SI4)	√(G2+R2)	0.42
Salinity Index5(SI5)	√(NIR*R)	0.39
Salinity Index6(SI6)	(B-R)/(B+R)	0.48
Salinity Index7(SI7)	(G*R)/G	0.36
Salinity Index8(SI8)	(B*R)/G	0.37
Salinity Index9(SI9)	√(G+R)	0.32
Salinity Index10(SI10)	B/R	0.37
Salinity Index11(SI11)	(R*NIR)G	0.38
Normalized Difference Vegetation Index(NDVI)	(NIR-R)/(NIR+R)	0.19
Spectral Response Index1(SRI1)	(B+G)/(R+NIR)*NDVI	0.96
Spectral Response Index2(SRI2)	(B+G)/(R+NIR)*SAVI	0.71

Table 3 .Summary of main statistical properties of soils and vegetation indices

median	maximum	minimum	Standard deviation	mean	point	variable
56.50	105	1.20	30.47	34.45	104	Salinity(ds/m)
7.80	8.20	7.10	0.28	7.73	104	Soil reaction(pH)
17.50	28.50	0.00	6.53	16.18	104	Calcium carbonate
0.26	0.57	-0.40	0.33	0.17	104	NDVI
1.23	0.45	-0.32	0.25	0.15	104	SAVI

NDVI was calculated for each sample, and the values ranged between -0.4 and 0.57 (Table 2). Values less than zero are related to bare soils and those higher than zero are related to sparse pasture vegetation, cotton crops, and barley fields. Pearson correlation coefficient (R) was used to determine the relationship of ECe with NDVI, SAVI, salinity indices, brightness index, and SRI. The correlation coefficient between salinity and index values ranged between 0.69 and -0.97. The minimum value belonged to normalized difference vegetation index, and the highest amount was related to the SRI1, combination of different vegetation indices, all blue, green, and red and Near Infrared bands. Different algorithms using spectral bands 1-4 were tested in combination with NDVI and SAVI. On the other hand, bare soil combined reflections were studied to determine the best communication with electrical conductivity. The correlation between salinity and NDVI index was exponentially reverse. With the increase in NDVI index values, the corresponding salinity values decreased exponentially. The correlation coefficient between soil salinity and NDVI index was low (-0.43) as the latter was affected by ground field reflecting. This means that ground field reflects the changes in the plant spectral behavior and reduces its spectral effect. Therefore, the SAVI index was examined. The relationship between this index and salinity indicated a higher correlation coefficient (-0.53) compared to that of salinity and NDVI. Various relationships have been studied to involve plant and soil reflection in salinity relationships and indices. Results of this study according to the findingsof Bouaziz *et al*. (2011) and Fan *et al*. (2012) whofound that SAVI, NDVI, and EVI vegetation indices were poorly correlated with EC values due to insufficient vegetation cover density while the soil salinity indices were more strongly correlated with the EC values.

The final algorithm is SRI (Spectral Response Index), which is expressed for a combination of bare soil and vegetation spectral reflections. The correlation coefficient between salinity and the values of SRI1 and SRI2 indices varied from-0.84 to -0.97. This shows the high capability of these two models in estimating salinity and providing a salinity map in scattered vegetation areas of salty and salt-resistant plants. Studying the relationship between salinity and various indices, the correlation coefficients indicated a significant relationship between SRI_1 and ECe values (Figure 3).

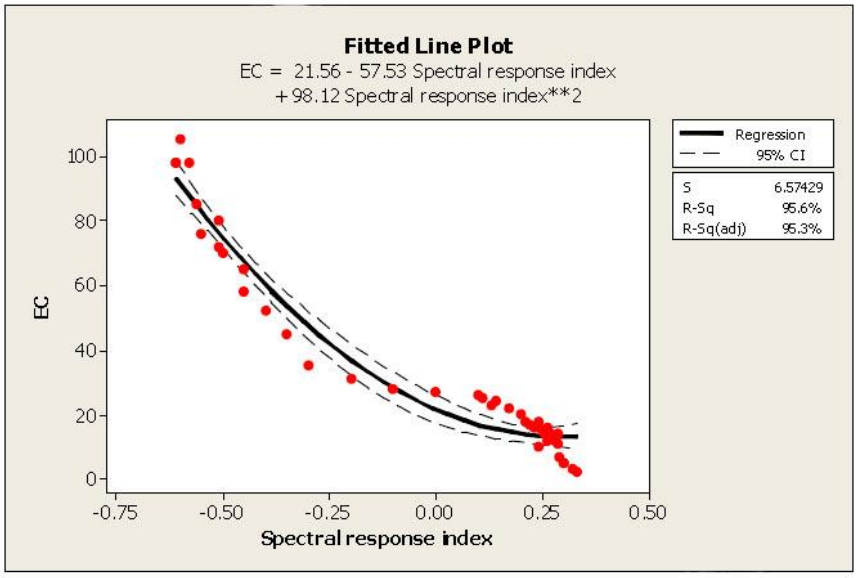

Fig. 3. Diagram of the relationship between salinity and the reflective composition of visible boundary and near infrared band index

The fitting model on salinity data exponential distribution and SRI index in a two-dimensional space is as follows:

$$EC = 21.56 - 57.53\ SRI_1 + 98.12\ SRI_1 \wedge 2 \qquad (1)$$

The result of implementing model 1 on SRI index of salinity map (Fig. 4). As observed, northern and northeastern regions had the minimum amount of vegetation and SAVI index with the maximum salinity values. Areas of irrigated crops such as corn, cotton and gardens had the minimum salinity because waterlogging washed away the salts from soil profiles, causing minimum amounts of saline on the soil surface. Therefore, the salinity in these areas is maintained at 2 to 6 ds/m. The results of matching salinity map of the model (1) with measured points confirming the authenticity of which can be measured with high reliability and users will benefit from these results. These high reflection characteristics of strongly saline soil (presence of thick crust) were easily captured by satellite remote sensing and played a vital role in the remote monitoring of soil salinization in large areas (Abbas *et al*., 2013).

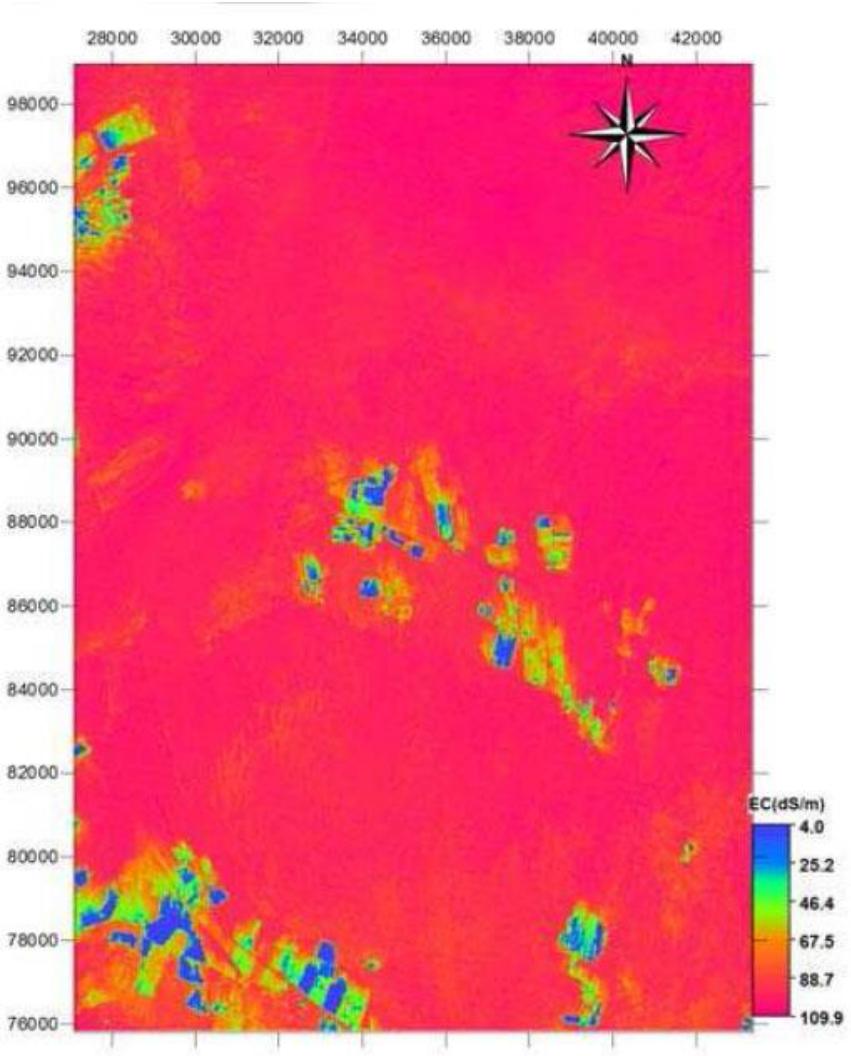

Fig. 4. Salinity map resulting from the model implementation

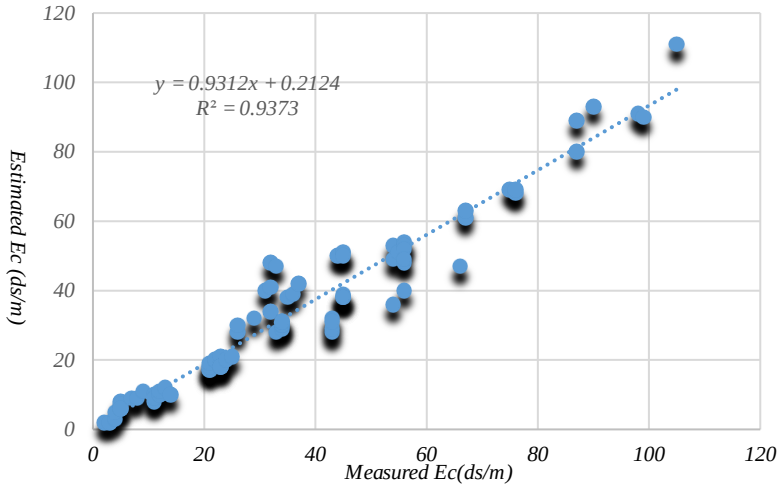

Fig. 5. Measured EC versus estimated EC through the best models performance

4. Conclusion

There was a good agreement between the estimated and measured EC (Fig. 5), and the model showed a very high correlation (R^2 = 0.93). Most parameters (blue, green, red and NIR and the vegetation index) indicateda good perception of the remote sensing data in the spatial mapping of soil salinity. Several works have been carried out on this topic. They have demonstrated the usefulness of satellite imagery in mapping, modeling, and spatial-temporal monitoring of soil salinity (El Hafyani *et al.*, 2019; Abdelrahman etal., 2019; Rahmaty M. and Hamzepoor N., 2017). Moreover, Albed *et al.* (2014) identified the NDSI and SAVI indices as the most suitable indices for the study of soil salinity in the Arabian Peninsula. Based on this and other sources, it is concluded that the accuracy of the indices for soil salinity measurement in each region varied according to the type and amount of soil salinity as well as the type of satellite data, which and should be studied and measured. Soil salinity of each area was further measured and calibrated.

References

Abbas, A., S. Khan, 2007. Using remote sensing techniques for appraisal of irrigated soil salinity. In: MODSIM 2007: International Congress on Modelling and Simulation: Land, Water and Environmental Management: Integrated Systems for Sustainability, pp. 2632–2638.

AbdelRahman M. A.E., M.M. Metwaly,A. Shalaby, 2019. Quantitative assessment of soil saline degradation using remote sensing indices in Siwa Oasis. Remote Sensing Applications: Society and Environment ,13.

Ahmed, I., H. Andrianasolo, 1997. Comparative assessment of multisensor data for suitability in study of the soil salinity using remote sensing and GIS in the Fordham irrigation division, Pakistan. In Proceedings of the Geoscience and Remote Sensing Symposium, Toronto, Canada, 4; 1627–1629.

Alavi Panah, S.K., M. De Dapper, R. Goossens, M. Massoudi, 2001. The use of Tm Thermal Band for Land Cover /Land Use Mapping in two different environmental conditions of Iran, JAST, 2;27-36.

Alavi Panah, SK., R. Goossens, M. De Dapper, 1999. Study of soil salinity in the Ardakan area, IRAN, based field observation and remote sensing, procceding of 8th EARSEL symposium NETHERLAND, May 1988

Allbed, A., L. Kumar, YY. Aldakheel, 2014. Assessing soil salinity using soil salinity and vegetation indices derived from IKONOS high-spatial resolution imageries: Applications in a date palm dominated region. Geoderma, 230; 1-8

Allbed, A., L. Kumar, P. Sinha, 2018. Soil salinity and vegetation cover change detection from multi-temporal remotely sensed imagery in Al Hassa Oasis in Saudi Arabia. Geocarto Int. 33 ; 830–846.

Asfaw, E., K.V. Suryabhagavan, M. Argaw, 2016. "Soil salinity modeling and mapping using remote sensing and GIS: The case of Wonji sugar cane irrigation farm, Ethiopia." Journal of the Saudi Society of Agricultural Sciences.

Ben-Dor, E., G. Metternicht, N. Goldshleger, E. Mor, V. Mirlas, U. Basson, 2008. Review of remote sensing based methods to assess soil salinity. In: Metternicht, G., Zaid, J.A. (Eds.), Remote Sensing of Soil Salinization: Impact on Land Management. CRC Press, Taylor and Francis, New York, pp. 39–56.

Bouaziz, M., J. Matschullat, R. Gloaguen, 2011. Improved remote sensing detection of soilsalinity from a semi-arid climate in Northeast Brazil. Compt. Rendus Geosci. 343; 795–803.

Brunner, P., W. Kinzelbach, H. Li, 2004. Generating large scale soil salinity maps with geophysics and remote sensing. Geophysical Research Abstracts 6; 04745.

Caccetta P.A., A. Allen, Watson, 2000. The land monitor project. In Proceedings of the 10th Australasian Remote Sensing and Photogrammetry Conference, Adelaide, Australia. Available at http://www.cmis.csiro.au/rsm/research/pdf/CaccettaP_lmpaper2000.pdf

Dwivedi, R.S., K. Sreenivas, 1998. Delineation of salt-affected and waterlogged areas in the Indo-

Gangetic,plains using IRS-1C LISS-III data.Int. J.Remote Sensing; 2739-2751.

Dwivedi, R., K. Ramana, S. Thammappa, A. Singh, 2001. The utility of IRS-1C, LISS-III and PANmerged data for mapping salt-affected soils. Photogrammetric Engineering and Remote Sensing, 67; 1167–1175.

El hafyani, M., A. Essahlaoui, M. El Baghdadi, C.T. Ana, M. Mohajane, A. El hmaidi, A. El ouali, 2019. Modeling and mapping of soil salinity in Tafilalet plain (Morocco). Arabian Journal of Geosciences, 12.

Eldeiry, A., L.A. Garcia, 2008. Soil sci. Soc. Am. J. Detecting soil salinity in alfalfa fields using spatial modeling and remote sensing, 72; 201–211.

Elhag, M., 2016. Evaluation of Different Soil Salinity Mapping Using Remote Sensing Techniques in Arid Ecosystems, Saudi Arabia." Journal of Sensors, 2016.

Fan, X., B. Pedroli, G. Liu, Q. Liu, H. Liu, L. Shu, 2012. Soil salinity development in the yellow river delta in relation to groundwater dynamics. Land Degrad. Dev, 23; 175–189.

Farifteh, J., A. Farshad, R.J. George, 2006. Assessing salt-affected soils using remote sensing, solute modelling, and geophysics. Geoderma, 130; 191-206.

Ferna´ ndez-Buces, N., C. Siebe, S. Cramb, J.L. Palacio, 2006. Mapping soil salinity using a combined spectral response index for bare soil and vegetation:A case study in the former lakeTexcoco, Mexico.65, Journal of Arid Environments.

Furby, S.L., J.F. Wallace, P. Caccetta, G.A. Wheaton, 1995. Detecting and monitoring saltaffected land: A report from the LWRRDC project detecting and monitoring changes in land condition through time using remotely sensed data. Remote Sensing and Image Integration Group, CSIRO Division of Mathematics and Statistics, Perth, WA, Australia. Available at http://www.cmis.csiro.au/rsm/research/Salmapmon/salmapmon_full.htm

Furby, S.L., R. Flavel, M. Sherrah, J. McFarlane, 1998. Mapping salinity in the Upper South East Catchment in SouthAustralia: A report fromthe LWWRDC projectmapping dryland salinity (CDM2). Remote Sensing and Image Integration Group, CSIRO Mathematical and Information Sciences,Western Australia.

Howari, F.M., 2003. The use of remote sensing data to extract information from agricultural land with emphasis on soil salinity. Australian Journal of Soil Research, 41;1243–1253.

Hick, P.T., W.G.R., Russell. 1988. Remote Sensing of Agricultural Salinity, WA. Remote Sensing Group, CSIRO Division of Exploration Geoscience, Western Australia.

Khan, N. M., V. Victor, Y. Rastoskuev, S. Sato, Shiozawa, 2005. Assessment of hydrosaline land degradationby using a simple approach of remote sensing indicators, Agricultural Water Management.

Khorram, S., S.A.C. Nelson, F.H. Koch, 2012. Remote Sensing. Springer

Kiiveri, H.T., P.A. Caccetta, 1998. Mapping salinity using decision trees and conditional probability networks. Digital Signal Processing, 8; 225–230.

McGowen, I., S. Mallyon, 1996. Detection of Dryland salinity using single and multi-temporal Landsat imagery. Proceedings of the 8t hAustralasian Remote Sensing Conference, Canberra, 26– 34).

Metternicht, G., J.A. Zinck, 2003. Remote sensing of soil salinity: Potentials and constraints. Remote Sensing of Environment, 85; 1–20

Metternicht, G., J.A. Zinck, 2008. Remote Sensing of Soil Salinization: Impact on Land Management. CRC Press, Taylor and Francis, New York.

Morshed, M. M., M. T. Islam, R. Jamil, 2016. "Soil salinity detection from satellite image analysis: an integrated approach of salinity indices and field data" Environmental Monitoring Assessment, 188: 119.

Mougenot, B., M. Pouget, G. Epema, 1993. Remote sensing of saltaffectedsoils. Remote Sensing Reviews, 7; 241–259.

Nagler, P., E.P. Glenn, A.R. Huete, 2001. Assessment of spectral vegetation indices for riparian vegetation in the Colorado River delta, Mexico. Journal of Arid Environments, 49; 91–110.

Rahmati, M., N. Hamzehpour, 2017. Quantitative remote sensing of soil electrical conductivityusing ETM+ and ground measured data International journal of remote sensing, 38.

Schmid, T., M. Koch, J. Gumuzzio, 2008. Applications of hyperspectral imagery to soil salinity mapping. In: Metternicht, G., Zaid, J.A. (Eds.), Remote Sensing of Soil Salinization: Impact on Land Management. CRC Press, Taylor and Francis, New York, 113–137.

Tamas, J., C. Lénart, 2006. Analysis of a small agricultural watershed using remote sensing techniques. Int. J. Remote Sensing, 27; 3727–3738.

Thomas, M., 2001. Remote sensing in South Australia's land condition monitoring project. Unpublished report, PIRSA Sustainable Resources, Land Information Group, Adelaide, Australia.

Verma, K.S., R.K. Saxena, A.K. Barthwal, S.N. Deshmukh, 1994. Remote sensing technique for mapping salt affected soils. International Journal of Remote Sensing, 15; 1901–1914.

Yan, G. U. O., Z. H. O. U. Yin, L. Q. ZHOU, L.I.U. Ting, L.G. WANG, Y.Z. CHENG, G.Q. ZHENG, 2019. Using proximal sensor data for soil salinity management and mapping. *Journal of integrative agriculture*, *18*; 340-349.

Zhang, T.T., S.L. Zeng, Y. Gao, Z.T. Ouyang, B. Li, C.M. Fang, B. Zhao, 2011. Using hyperspectral vegetation indices as a proxy to monitor soil salinity. Ecol. Indic, 11; 1552–1562.

Zinck, J.A., 2001. Monitoring salinity from remote sensing data. InR.Goossens, and B. M. De Vliegher (Eds.), 1st Workshop of the EARSeL Special Interest Group on Remote Sensing for DevelopingCountries, pp. 359– 368, Belgium: Ghent University. Hick P.T. and W.G.R. Russell. 1988. Remote Sensing of Agricultural Salinity, WA. Remote Sensing Group, CSIRO Division of Exploration Geoscience, Western Australia.